

Chapter 5

Protostars & pre-main-sequence evolution

We have discussed the structure and collapse of cold cores in the previous chapters without putting much emphasis on the protostellar core structure. We treated the central core as a sink of mass and only considered its gravitational impact on the outer envelope. It is however clear that this inner core will at some point start to irradiate the remaining envelope from the inside. Hence, in this chapter, we focus on the evolution and detailed structure of the protostar all the way from its formation to the arrival on the main-sequence.

5.1 Timescales

There are three timescales relevant for the protostar: (1) the free-fall timescale of the collapsing core, (2) the Kelvin-Helmholtz timescale, (3) the accretion timescale.

The free-fall timescale was derived in chapter 3

$$t_{\text{ff}} = \sqrt{\frac{3\pi}{32G\rho}} \approx \sqrt{\frac{1}{G\rho}} \quad , \quad (5.1)$$

and describes the time that a particle within a cloud of density ρ would take to fall a distance r (we approximated here $\sqrt{3/2\pi} = 0.7$ to be of the order of 1 since these types of estimates are order of magnitude estimates anyhow).

The second timescale has been introduced in chapter 1

$$t_{\text{KH}} = \frac{U_{\text{grav}}}{L_*} = \frac{3}{5} \frac{GM_*^2}{R_* L_*} \quad . \quad (5.2)$$

This describes the time that a star can radiate its luminosity L_* with the sole energy source being its gravitational energy U_{grav} .

The accretion timescale can be expressed as

$$t_{\text{acc}} = \frac{M_{\text{core}}}{\dot{M}} \quad . \quad (5.3)$$

The free-fall timescale is much shorter than the Kelvin-Helmholtz timescale and the accretion timescale. Comparing the latter two, we can distinguish two cases, $t_{\text{KH}} > t_{\text{acc}}$ and $t_{\text{KH}} < t_{\text{acc}}$. In the first case, the stellar interior cannot thermally adjust to the accretion and the luminosity will be generated by accretion shocks on the surface (dissipation of kinetic energy into heat). This is the 'protostellar phase'. In the latter case, the accretion becomes inefficient and the star evolves towards the main-sequence on a thermal timescale with the stellar luminosity being generated by contraction. We call this the 'pre-main sequence phase'.

If we consider the expression for the mass accretion rate that follows from the simple Shu inside-out collapse model, we can estimate the value of accretion rates as well as the timescale for forming a $1 M_{\odot}$ star from an isothermal 10 K envelope

$$\dot{M} \sim \frac{c_s^3}{G} \sim 1.6 \times 10^{-6} M_{\odot} \text{ yr}^{-1} \quad (5.4)$$

$$t_{\text{acc}} = 6.3 \times 10^5 \text{ yr} . \quad (5.5)$$

5.2 Early growth and collapse

The isothermal approximation that we used in the previous section for the core collapse breaks down when we consider the forming protostar itself. Initially, the temperature of the core is fairly low, a few 100–1000 K, and thus most of the energy will be radiated in the infrared. As material piles up on the central core, the matter rapidly becomes optically thick, thus preventing gravitational energy from being efficiently radiated away. This leads to an increase in central temperature and the growing gas pressure acts to stabilize the core (Fig. 5.1). The core continues to grow until it reaches a mass of $\sim 5 \times 10^{-2} M_{\odot}$; it has then a size of roughly 5 AU.

From the simplest form of the virial theorem (only thermal and gravitational energy, no magnetic and kinetic energy)

$$\begin{aligned} U_{\text{grav}} &= -\frac{3}{5} \frac{GM_*^2}{R_*} \\ &= -2U_{\text{therm}} = -2 \frac{3}{2} \frac{kTM_*}{\mu m_{\text{H}}} , \end{aligned} \quad (5.6)$$

we can derive an estimate for the temperature

$$T = \frac{m}{5k} \frac{GM_*}{R_*} \approx 520 \text{ K} \left(\frac{M_*}{5 \times 10^{-2} M_{\odot}} \right) \left(\frac{R_*}{5 \text{ AU}} \right)^{-1} \quad (5.7)$$

Here, M_* and R_* denote the mass and radius of the protostellar core. We have assumed a mean molecular weight $\mu = 2.4$ appropriate for molecular gas.

In this first phase, molecular hydrogen acts as a thermostat. At temperatures above 2000 K, collisions can dissociate H_2 , a process that absorbs 4.48 eV. At the same time, the thermal energy of an H_2 molecule is only 0.74 eV. Hence, during this phase, most of the gravitational contraction energy can be absorbed through the dissociation of a small fraction of the total molecular hydrogen. As a consequence, the temperature rise becomes more moderate as also shown in Fig. 5.1. The central region with atomic hydrogen starts to spread outward and this eventually leads to an unstable configuration as the adiabatic index drops below the critical value of 4/3.

As the density rises further $\rho \sim 10^{-2} \text{ g cm}^{-3}$, hydrogen can eventually be ionized, thus pushing the adiabatic index beyond 4/3. This leads to the formation of a second stable core which grows to $0.01\text{--}0.02 M_{\odot}$ in less than 100 yr.

The protostellar mass then grows to its final value during the main accretion phase, or ‘protostellar phase’, where $t_{\text{acc}} < t_{\text{KH}}$. We can estimate the maximum size that a protostar can have as well as its accretion

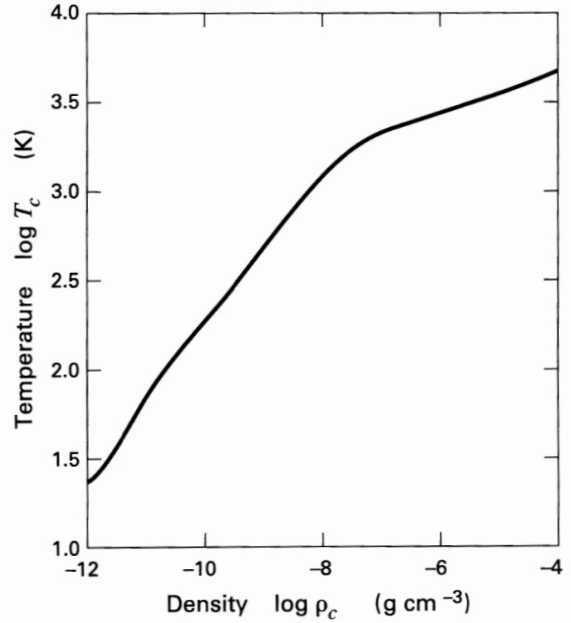


Figure 5.1: Evolution of the central temperature in the first core. The temperature is plotted as a function of central density (from Stahler & Palla 2004).

luminosity again from simple consideration of the virial theorem $U_{\text{therm}} = -1/2 U_{\text{grav}}$, we can write down the energy conservation equation as

$$-\frac{1}{2} \frac{3}{5} \frac{GM_*^2}{R_*} + E_{\text{int}} + L_{\text{rad}} t = 0 , \quad (5.8)$$

where L_{rad} is the average luminosity escaping over the timescale t and E_{int} is the internal energy of the gas. Since the matter is initially in a cold sphere with large dimensions, the initial internal energy can be considered to be zero. However, during the contraction, molecular hydrogen gets dissociated (dissociation energy $E_{\text{diss}} = 4.48$ eV) and hydrogen and helium get ionized (ionization energies $E_{\text{ion}}(\text{H}) = 13.6$ eV and $E_{\text{ion}}(\text{He}) = 75$ eV). We can consider this as internal energy ΔE_{int} which we can thus write as

$$\Delta E_{\text{int}} = \frac{XM_*}{m_{\text{H}}} \left[\frac{\Delta E_{\text{diss}}(\text{H}_2)}{2} + \Delta E_{\text{ion}}(\text{H}) \right] + \frac{YM_* \Delta E_{\text{ion}}(\text{He})}{4m_{\text{H}}} . \quad (5.9)$$

X and Y are here the mass fractions of hydrogen and helium respectively. If we ignore L_{rad} , we can derive an expression for the maximum possible radius of the protostar

$$R_{\text{max}} = \frac{3}{10} \frac{GM_*^2}{\Delta E_{\text{int}}} = 36 R_{\odot} \left(\frac{M_*}{M_{\odot}} \right) . \quad (5.10)$$

The observed sizes of e.g. T Tauri stars (solar mass protostars) are generally smaller by an order of magnitude.

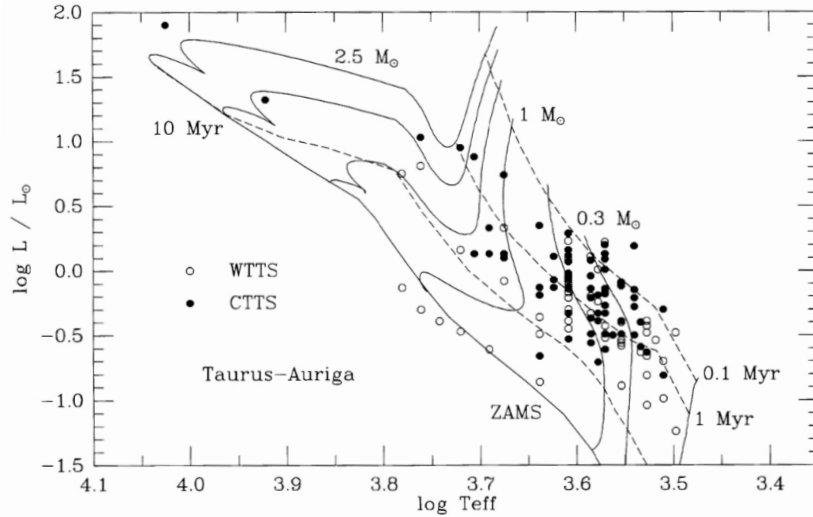


Figure 5.2: HR diagram positions of young stars lying within the Taurus-Auriga molecular cloud complex. For comparison, theoretical evolutionary tracks for pre-main-sequence stars of masses 2.5, 2.0, 1.5, 1.0, 0.5, 0.3, and 0.1 M_{\odot} are shown. The dashed lines are isochrones for ages of 10^5 , 10^6 , and 10^7 yr with the hydrogen-fusion zero-age main sequence (ZAMS) shown as the lowest line running from upper left to lower right. The open circles refer to weak-emission T Tauri stars (WTTS), while the filled circles denote the position of the classical T Tauri stars (CTTS) (figure and caption from Hartmann 1998).

Since we know that the true stellar radius is much smaller than the derived estimate of R_{max} , we know that the second term in Eq.(5.8) must be much smaller than the first one (if $R = R_{\text{max}}$, the two terms would be equal). Hence, we can neglect the second term in Eq.(5.8), ΔE_{int} and derive an expression for the

luminosity which we assume to be close to the accretion luminosity

$$L_{\text{acc}} = \frac{3}{10} \frac{GM_*}{R_*} \dot{M} \quad (5.11)$$

$$\approx 18 L_{\odot} \left(\frac{\dot{M}}{10^{-5} M_{\odot} \text{ yr}^{-1}} \right) \left(\frac{M_*}{M_{\odot}} \right) \left(\frac{R_*}{5 R_{\odot}} \right)^{-1} \quad (5.12)$$

For this, we assumed that $\dot{M} = M_*/t$. This equation tells us, that for a protostar with a fixed mass M_* , the energy loss through radiation will directly be connected to a contraction. If we assume for a second that the temperature of the star will stay constant (e.g. at a reference point in time, the star has the size R_0 and luminosity L_0),

$$L_* = 4\pi R_*^2 \sigma T_*^4 \quad (5.13)$$

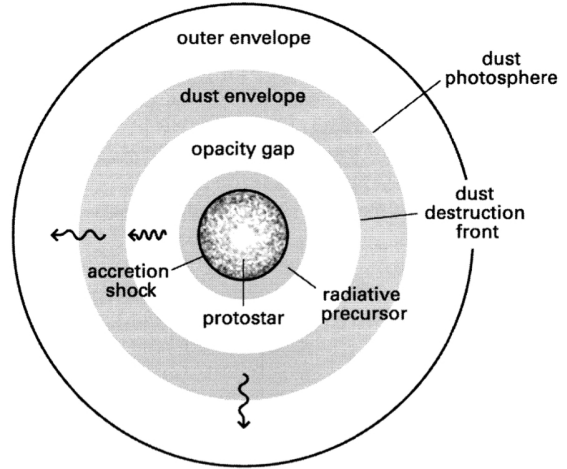
$$T_* = \left(\frac{L_*}{4\pi\sigma R_*^2} \right)^{1/4} \approx \text{constant} \quad (5.14)$$

$$L_* = L_0 \frac{R_*^2}{R_0^2} \quad (5.15)$$

$$L_* = L_0 \left(\frac{7}{3} \frac{t L_0 R_0}{GM_*^2} \right)^{-2/3} = L_0 \left(\frac{7}{5} \frac{t}{t_{\text{KH}}} \right)^{-2/3} \quad (5.16)$$

As the star ages, it becomes thus smaller and fainter. The rate of change in luminosity and size slows with age. This is illustrated in Fig. 5.2, where the pre-main-sequence evolutionary tracks are shown in an HR diagram. The almost vertical part of the evolutionary track ($T_* \approx \text{constant}$) is frequently referred to as 'Hayashi track'. A protostar is often defined as an object that derives most of its luminosity from accretion, hence $L_* \sim L_{\text{acc}}$.

At this point, we make a small note concerning some of the pre-factors in all these equations. Depending of which book one consults, these factors can differ by factors of π , 2 or 4, or anything close to it. Most of the time, these differences are irrelevant since the equations themselves contain assumptions that are often only order of magnitude assumptions. Hence, a factor 2 is never a problem. However, if you ever encounter larger discrepancies, please consult one of the authors (lecturers) to resolve the issue. It could very well be a typo. Within this syllabus, we try to be as consistent as possible in the definitions of certain quantities such as Kelvin-Helmholtz timescale, Jeans radius etc..



5.3 Dust envelope

We have now derived expressions for the luminosity and size of a protostar, but these are rather theoretical quantities as the surrounding envelope of material often is optically thick at UV and optical wavelength and starts to become more transparent in the infrared (see dust opacity as a function of wavelength). This means the actual surface of emission is not the protostar itself, but rather a sort of dust photosphere that we will now explore in somewhat

Figure 5.3: Structure of a spherical protostar and its infalling envelope. The relative dimensions of the outer regions have been greatly reduced in this sketch. Note the conversion from optical to infrared photons in the dust envelope (figure and caption from Stahler & Palla 2004).

more detail (Fig. 5.3). It also means that the UV/optical photons of the star are absorbed and scattered many times in the envelope and heat the dust there to a temperature T_{dust} . The envelope dust then emits according to its own temperature, mostly in the infrared. Hence, stellar photons are converted into infrared photons emitted by the dust. The dust photosphere is then the layer where most of the emission is coming from, hence the $\tau_{\text{R}} \sim 1$ layer (analogy to the solar photosphere at optical wavelength; τ_{R} is the Rosseland mean optical depth).

We can find an estimate for the size of this dust photosphere by using the following two equations

$$\rho(r)\kappa_{\text{R}}R_{\text{phot}} = 1 \quad (5.17)$$

$$L_{\text{acc}} = 4\pi R_{\text{phot}}^2 \sigma T_{\text{phot}}^4, \quad (5.18)$$

where κ_{R} is the Rosseland mean opacity, ρ is the density profile found from the inside-out collapse for the free-fall region, and T_{phot} , R_{phot} are the temperature and radius of the dust photosphere. Numerical solution of this system of two equations with two unknowns yields values of $R_{\text{phot}} = 2.1 \times 10^{14}$ cm (14 AU) and $T_{\text{phot}} = 300$ K. So, according to Wien's law, the peak emission lies indeed in the infrared spectral region (around $50 \mu\text{m}$). Of course, these mean opacities and simple approximations can only give a very crude picture of what the dust photosphere is. Full frequency-dependent radiative transfer is needed to calculate the dust temperature through an iterative (the local source function depends on the dust temperature and vice versa) or Monte-Carlo procedure.

5.4 Stellar structure

After this short excursion into the outer envelope, we now return to the protostellar interior and study the stellar structure equations that will tell us how mass and radius are related for these objects (similar to the mass-radius relation for main-sequence stars). We then discuss deuterium burning and lithium destruction in the stellar interior.

The basic equations of stellar structure are the equations of mass continuity, hydrostatic equilibrium, state, energy transport and energy generation

$$\frac{\partial M_r}{\partial r} = 4\pi r^2 \rho(r) \quad (5.19)$$

$$\frac{\partial P}{\partial r} = -\frac{G\rho(r)M_r}{r^2} \quad (5.20)$$

$$P(r) = \frac{\rho(r)}{\mu} RT \quad (5.21)$$

$$\frac{\partial T_r}{\partial r} = L_r \left[\frac{\kappa\rho(r)}{16\pi r^2 \sigma T_r^3} \right] \quad (5.22)$$

$$\frac{\partial L_{\text{int}}}{\partial r} = 4\pi r^2 \rho \left(\epsilon(r) - T \frac{\partial s}{\partial t} \right) \quad (5.23)$$

where R is the gas constant, μ the mean molecular weight, $\epsilon(r)$ the rate of nuclear energy generation per unit mass within a shell of size r and s the specific entropy (entropy per units mass). The second term in the energy generation $-T\partial s/\partial t$ stems from the contraction of the star.

We can solve these equations numerically by using opacities, mean molecular weights, energy generation rate and entropy tabulated as functions of T and ρ . To close the systems of equations, we also need some boundary conditions. For the center of the protostar, M_r and L_{int} vanish

$$M(0) = 0 \quad (5.24)$$

$$L_{\text{int}}(0) = 0. \quad (5.25)$$

At the surface of the protostars $r = R_*$, the pressure should approach the ram pressure of the infalling gas

$$P = \rho v_{\text{ff}}^2 = \frac{\dot{M} R_*^{-3/2}}{4\pi \sqrt{2GM_*}} \frac{2GM_*}{R_*} = \frac{\dot{M}}{4\pi} \cdot \left(\frac{2GM_*}{R_*^5} \right)^{1/2} \quad (5.26)$$

The last boundary condition concerns the protostars luminosity, which should be the sum of the accretion luminosity and internal luminosity (see last of Eq.(5.23))

$$L_* = L_{\text{acc}} + L_{\text{int}} . \quad (5.27)$$

5.4.1 Mass-radius relation

To understand pre-main sequence stellar evolutionary tracks, we like to follow the mass and radius of our protostar from the start. Initial conditions for integrating Eqs.(5.23) vary widely and so in the beginning, the solutions diverge. However, after the first doubling of the mass, the solutions are indistinguishable (see Fig. 5.4).

It is also important to note that low mass protostars (T Tauri stars) are fully convective (grey area) while higher mass protostars do form a radiative core. To understand this, we have to recall that the main opacity source in the photosphere of these protostars, H^- , is highly dependent on temperature (for $T < 10^4$ K). The temperature dependance of the opacity is thus a sort of valve that regulates the surface temperature of the star. For a fixed mass and radius, there is a minimum allowed T_{eff} , called Hayashi temperature, implying also a minimum stellar luminosity. On the other hand, there is a maximum luminosity that can be transported by radiation (L_{crit}). When the minimum stellar luminosity according to the Hayashi temperature exceeds (L_{crit}), the protostar becomes quickly fully convective. This is the case for low mass protostars. Higher mass protostars, $2 - 8 M_{\odot}$, have a luminosity that exceeds (L_{crit}) and thus they can sustain a radiative core.

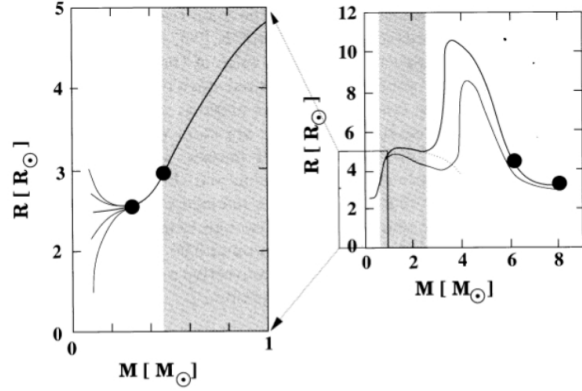


Figure 5.4: Evolution of stellar radius with mass using a constant accretion rate of $10^{-5} M_{\odot}/\text{yr}$. The left figure illustrates low mass pre-MS stars, the right one the entire mass range up to $8 M_{\odot}$. The grey area indicates where the protostars are fully convective; black dots mark the onset of deuterium burning, the point where stars are fully convective, the ignition of hydrogen in the core, and the arrival at the ZAMS. The thin line in the right panel illustrates the use of different boundary conditions (figure from Schulz 2004).

5.4.2 Deuterium burning

Deuterium is one of the elements generated in the Big Bang with a primordial abundance of $[D/H] = 3 - 5 \times 10^{-5}$. It starts burning at temperatures above 10^6 K. In low mass stars, $< 1 M_{\odot}$, mass accretion provides a steady supply of new deuterium fuel and the fusion process itself drives the protostars convection, thereby mixing the newly accreted fuel down into the core. The total amount of energy available from deuterium burning equals the gravitational energy of the protostar. Thus, deuterium regulates in that stage the mass-radius relation of the protostar (this depends on the mass accretion rate).

For higher mass stars, $M > 2 M_{\odot}$, the deuterium fusion depletes the core. Since new material is still accreting, the deuterium burning continues in a shell.

5.4.3 Lithium destruction

If the temperature in the core of the protostar reaches $\sim 2.5 \cdot 10^6$ K, Li-burning consumes ${}^7\text{Li}$ (the dominant isotope) through the reaction ${}^7\text{Li}(p, \alpha){}^4\text{He}$. The interstellar medium Li abundance is $[Li/H] \sim 2 \cdot 10^{-9}$, which is about an order of magnitude higher than the primordial value.

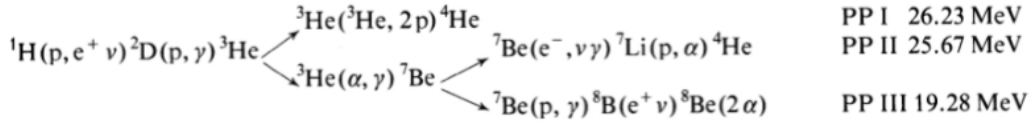
Low mass protostars never reach the central temperatures necessary for Li-burning, while more massive ones quickly exhaust their Li in the core. If the star has a mass $< 0.9 M_{\odot}$, it is fully convective during this period and hence destroys his entire Li reservoir. More massive stars cease to be fully convective before

all Li is consumed. Stars more massive than $1.2 M_{\odot}$ only have shallow convection zones and hence do not deplete their Li significantly.

Measuring the Li abundance in young clusters can hence serve as a powerful test of pre-main-sequence stellar structure and evolution theory.

5.4.4 Hydrogen ignition

When deuterium burning ceases in the core, the star once more contracts gravitationally til it reaches a core temperature of 10^7 K. At those temperatures four protons can fuse into a ^4He atom. During this process, two of the four protons decay into neutrons. The process is known as the pp-chain



At temperatures larger than $1.5 \cdot 10^7$ K, the CNO cycle takes over converting most of the initial C, N, and O into ^{14}N .

5.5 Magnetospheric accretion

Magnetic fields and rotation largely determine the accretion flow as outlined in the previous chapter (Sects. 4.2.4 and 4.2.5) and lead to the formation of an accretion disk. In the initial short collapse phase, accretion is dominated by envelope accretion onto the star. However, in later stages follows a much longer phase of disk accretion. In the latter phase, the accretion flow is predominantly through the disk onto the central protostar.

5.5.1 Theory

Within the accretion disk, angular momentum is transported — via some poorly understood viscosity — from the inner disk outwards to a small fraction of disk mass, so that the inner disk effectively loses angular momentum, while the outer disk gains some. This enables mass accretion from the inner disk onto the protostar and leads at the same time to a viscous spreading of the disk. Fig. 5.5 illustrates schematically how angular momentum is transported in a shearing disk. The angular velocity is decreasing outwards. If there is friction or communication between two neighboring annuli, the resulting torques will try to bring them into corotation. This accelerates gas in the outer annulus, while it decelerates gas in the inner annulus. Hence, the inner annulus loses angular momentum to the outer one. The same happens in the presence of a magnetic field, where we can illustrate the effect in form of an elastic spring connecting the two annuli. As the inner one rotates slower, the spring will be stretched out, thereby causing the inner annulus to break and lose angular momentum.

In a two-dimensional gaseous disk, angular momentum will be transported by turbulent motions, that is gas being mixed by turbulence among different annuli. This works as long as there is shearing orbital motion, $d\Omega/dR \neq 0$. Possible sources of turbulent motions are magnetic fields and convection. An alternative process for angular momentum transport are gravitational instabilities. We will get back to the details of angular momentum transport, viscosity and disks in a later chapter.

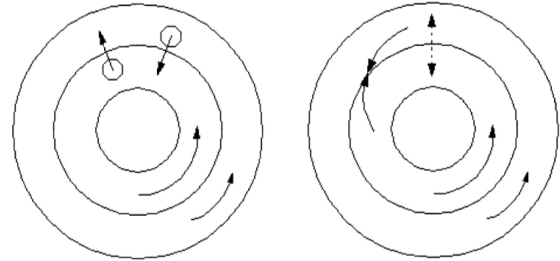


Figure 5.5: Schematic view of angular momentum transport in a shearing disk.

5.5.2 Observations

As material accretes from the disk onto the star, it hits the stellar surface, thus forming an accretion shock. Within the magnetospheric accretion model, the material flows along so-called funnel flows shaped by the connection of the stellar magnetic field with the disk (Fig. 5.6 and 5.10). The disk is truncated at a distance of several stellar radii. The accretion rates can be measured by looking at the veiling of the stellar spectrum (spectral lines) due to the accretion layer above (see also Fig. 5.9).

The stellar absorption lines will be partially filled in by the continuum emission from the hot accretion layer. By measuring this effect in a spectral line and the adjacent continuum, we can estimate the veiling r defined as the ratio between the excess F^E and stellar fluxes F_c^* as

$$r = \frac{F_l^o/F_c^o - F_l^*/F_c^*}{1 - F_l^o/F_c^o} \quad (5.28)$$

where l and c refer to the line and continuum of the veiled object (o) or the stellar photosphere ($*$) (Gullbring 1998). In this way, we can estimate the excess hot continuum emission and estimate its total luminosity L_{hot} . This luminosity is related to the accretion rate in the following way

$$L_{\text{hot}} \approx \frac{GM_* \dot{M}}{R_*} \left(1 - \frac{R_*}{R_m}\right) \quad (5.29)$$

where R_m is inner radius of the disk, the magnetospheric radius, i.e. the radius where the magnetic field of the star truncates the disk. Thus by obtaining high resolution spectra of young stars, we can estimate their accretion rates. Given the uncertainties in the details of the accretion process, these estimates should be considered as order of magnitude estimates.

5.6 Evolution in the HR diagram

In the previous section, we described how we can obtain the radius, mass and luminosity of the protostar (pre-main sequence star). Fig. 5.7 illustrates now the evolutionary track that pre-main sequence stars of various masses take before they reach the hydrogen burning stage, the zero-age main sequence (ZAMS, thick dashed line). Low mass stars of $0.5 M_\odot$ take 160 Myr to reach the

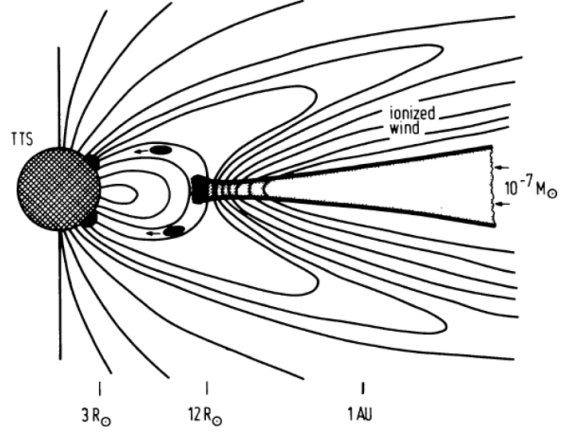


Figure 5.6: A sketch of the basic concept of magnetospheric accretion in T Tauri stars (from Camenzind 1990).

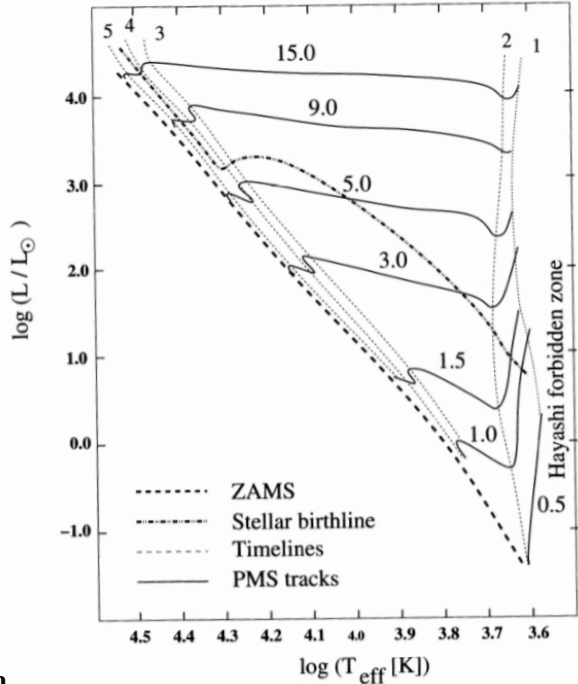


Figure 5.7: Evolutionary path in the HR diagram. Thin dashed lines indicate timelines labelled 1, 2, 3, 4, and 5. Timeline 1 is the beginning of the Hayashi track, timelines 2-5 cover the radiative track of the HR-diagram. The thick dashed line is the zero-age main sequence; the thick dash-dotted line the stellar birthline for an accretion rate of $10^{-5} M_\odot/\text{yr}$ (figure from Schulz 2004).

ZAMS, solar mass stars 50 Myr, and higher mass stars

($3 M_\odot$) only 2.5 Myr.

5.6.1 Birthline

When protostars begin their quasi-hydrostatic contraction towards the ZAMS, they become optically visible. The location where this happens in the HR diagram is a well-defined line called the birthline. The star has then more or less reached its final mass. In principle, this location should coincide with the location of the youngest pre-main sequence stars observed in star forming regions. However, it depends on the assumed mass accretion rate (in the figure, this is $10^{-5} M_{\odot}/\text{yr}$), with higher accretion rates shifting the line upward.

5.6.2 Hayashi tracks

We have encountered earlier the finding of Hayashi (1966) that a protostar of a certain radius and mass has a minimum effective temperature, the Hayashi temperature. For temperatures lower than that, the protostar is not stable and will tend to drift back to a stable configuration. The Hayashi tracks in the HR diagram mark thus asymptotes to these instabilities. As noted earlier, low mass protostars have extended Hayashi tracks, while higher mass protostars develop a radiative core and have thus very short or no Hayashi track.

5.7 PMS classification

Fig. 5.8 provides an overview of the various evolutionary phases of star and disk formation in the context of object classification, physical and observational properties. In the following, we discuss briefly four classes of pre-main sequence objects, three low mass object types, the classical T Tauri, weak line T Tauri, and FU Orionis stars and the intermediate mass object type, the Herbig AeBe stars.

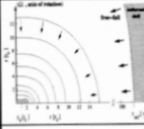
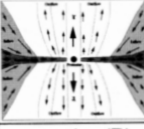

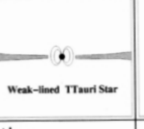
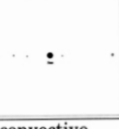
	Infalling protostar	Accreting protostar	Contracting PMS star		MS star
YSO properties					
Phase	adiabatic (A,B,C)	accretion (D) deuterium burning onset of convection	convective radiative onset of nuclear burning		convective radiative full nuclear burning
Matter flows	mostly infall disk & outflows form	some infall mostly accretion outflows, jets	low accretion	?	—
Envelope/ disk size	< 10000 AU	< 1000 AU	< 400 AU	~ 100 AU	—
Infall/ accretion rate	10^{-4}	10^{-5}	10^{-6} -- 10^{-7}	?	—
Age	10^4 - 10^5 yr	10^5 yr	10^6 -- 10^7 yr	10^6 -- 10^7 yr	—
Emission bands (except IR)	thermal radio X-ray?	radio X-ray	radio optical strong X-ray	non-therm. radio optical strong X-ray	non-therm. radio optical X-ray
Classes	Class 0	Class I	Class II	Class III	ZAMS

Figure 5.8: The IR classification in the context with evolutionary phases and matter flow parameters (figure and caption from Schulz 2005).

5.7.1 T Tauri stars

Classical T Tauri stars (CTTS) are named after the prototype T Tau in the Taurus star forming region. Characteristics are strong Balmer line emission ($H\alpha$), and an association with reflection nebulae and molecular clouds. These stars are low-mass pre-main sequence stars with spectral types between F and M and effective temperatures ranging from 3000 to 7000 K. They are class II sources according to their SED and the IR excess peaks between 1 and 10 μm . The median disk mass is $0.01 M_{\odot}$ with a huge spread around it ($0.0003 - 1 M_{\odot}$). Typical disk radii are around 100 AU (see Fig 5.10 for a sketch of the star-disk system). Accretion shocks and stellar activity (coronal heating) produce strong X-rays with luminosities up to $L_X = 10^{31} \text{ erg s}^{-1}$. Here, accretion shocks in the free-falling flow contribute mostly to the soft X-rays, while accretion shocks on the surface only produce excess far UV radiation (see Fig. 5.9).

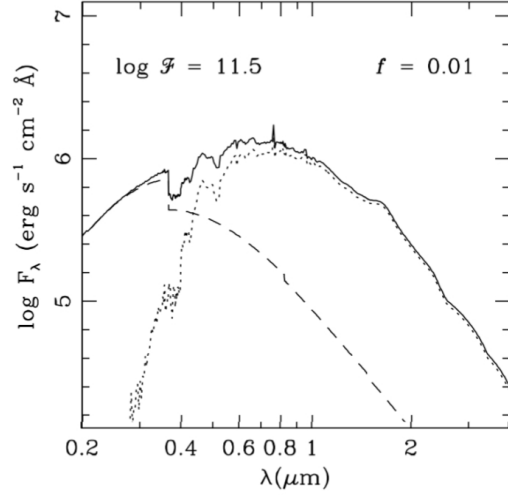


Figure 5.9: The the total spectral energy distribution (solid line) of a K7-M0 photosphere (dotted line) plus excess continuum (dashed line) for a value of $\log F = 11.5 = \log (L_{\text{acc}}/(fR_*^2))$ and a filling factor $f = 0.01$ (adapted from Calvet & Gullbring 1998).

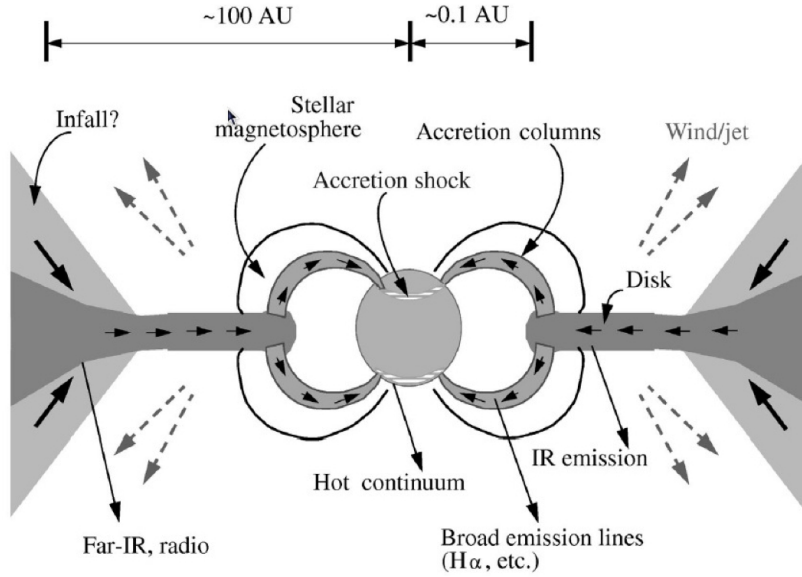


Figure 5.10: Schematic picture of accretion in T Tauri stars. The pre-main sequence star is surrounded by accreting circumstellar disk which emits at infrared, sub-mm and mm wavelength. The inner disk is disrupted by stellar magnetic field, which cause accreting material to be diverted out of the disk and fall rapidly onto the star. This magnetospheric material emits broad emission lines as it falls along the accretion columns, and produces a hot continuum when it crashed into the stellar surface at an accretion shock (figure and caption from Hartmann 1998)